

Characterization of the Bis-Silylated Endofullerene Sc₃N@C₈₀

Takatsugu Wakahara,[†] Yuko Iiduka,[†] Ozora Ikenaga,[†] Tsukasa Nakahodo,[†]
 Akihiro Sakuraba,[‡] Takahiro Tsuchiya,[†] Yutaka Maeda,[§] Masahiro Kako,^{||}
 Takeshi Akasaka,^{*,†} Kenji Yoza,[⊥] Ernst Horn,[#] Naomi Mizorogi,[@] and
 Shigeru Nagase^{*,@}

Contribution from the Center for Tsukuba Advanced Research Alliance, University of Tsukuba, Tsukuba, Ibaraki 305-8577, Japan, Graduate School of Science and Technology, Niigata University, Niigata, Niigata 950-2181, Japan, Department of Chemistry, Tokyo Gakugei University, Koganei, Tokyo 184-8501, Japan, Department of Applied Physics and Chemistry, The University of Electro-Communications, Chofu, Tokyo 182-8585, Japan, Bruker AXS K.K., Yokohama, Kanagawa 221-0022, Japan, Department of Chemistry, Rikkyo University, Tokyo 171-8501, Japan, and Department of Theoretical Molecular Science, Institute for Molecular Science, Okazaki, Aichi 444-8585, Japan

Received April 2, 2006; E-mail: akasaka@tara.tsukuba.ac.jp

Abstract: The photochemical reaction of Sc₃N@C₈₀ with 1,1,2,2-tetramesityl-1,2-disilirane affords the adduct as a bis-silylated product. The adduct was characterized by NMR spectroscopy and single-crystal X-ray structure analysis. The dynamic behavior of the disilirane moiety and the encapsulated Sc₃N cluster were also investigated. The unique redox property of the adduct is reported by means of CV and DPV. Experimental results were confirmed by density functional calculations.

Introduction

Endohedral metallofullerenes have attracted significant interest due to their novel properties resulting from their special molecular structures.^{1–3} To date many endohedral fullerenes have been prepared and isolated. Dorn et al. have developed a new synthetic method to afford a novel endohedral metallofullerene, namely Sc₃N@C₈₀.⁴ Splendidly, the quantity of Sc₃N@C₈₀ obtained exceeds that of the abundant empty C₈₄, which is the third most abundant fullerene, next to C₆₀ and C₇₀, under normal conditions.⁵ Density functional calculations confirm the stability of Sc₃N@C₈₀.⁶ Since Sc₃N@C₈₀ can be isolated in a remarkably high yield, the design of Sc₃N@C₈₀ derivatives has a considerable potential for their applications in material science and biochemistry. Dorn and co-workers

reported the NMR spectral and X-ray crystal data of a Diels–Alder monoadduct of Sc₃N@C₈₀, which is the only completely characterized derivative of this endohedral metallofullerene.^{7a}

Exohedrally derivatized endohedral metallofullerenes are very interesting for their potential usefulness as novel materials. The study of derivatization of metallofullerenes is almost completely based on the introduction of a carbon group.⁷ Meanwhile, organosilicon compounds represent a unique feature of materials.⁸ In a series of our studies of the chemical functionalization of fullerenes with organosilicon compounds,⁹ we have reported the bis-silylation of metallofullerenes with 1,1,2,2-tetramesityl-1,2-disilirane (hereafter abbreviated as disilirane)¹⁰ as well as C₆₀ and higher fullerenes.¹¹ Addition of disilirane can tune the electronic properties of metallofullerenes; the cages of silylated metallofullerenes become electron-rich as a result of the electron donation from the disilirane moiety. Very recently, we revealed the chemical reactivity of Sc₃N@C₈₀ with disilirane from the

[†] University of Tsukuba.

[‡] Niigata University.

[§] Tokyo Gakugei University.

^{||} The University of Electro-Communications.

[⊥] Bruker AXS K.K.

[#] Rikkyo University.

[@] Institute for Molecular Science.

- Heath, J. R.; O'Brien, S. C.; Liu, Y.; Curl, R. F.; Kroto, H. W.; Title, F. K.; Smalley, R. E. *J. Am. Chem. Soc.* **1985**, *107*, 7779–7780.
- Chai, Y.; Guo, T.; Jin, C.; Haufler, R. E.; Chibante, L. P. F.; Fure, J.; Wang, L.; Alford, J. M.; Smalley, R. E. *J. Phys. Chem.* **1991**, *95*, 7564–7568.
- Endofullerenes: A New Family of Carbon Clusters*; Akasaka, T., Nagase, S., Eds.; Kluwer: Dordrecht, The Netherlands, 2002.
- Stevenson, S.; Rice, G.; Glass, T.; Harich, K.; Cromer, F.; Jordan, M. R.; Craft, J.; Hadju, E.; Bible, R.; Olmstead, M. M.; Maitra, K.; Fisher, A. J.; Balch, A. L. *Nature* **1999**, *401*, 55–57.
- Krätschmer, W.; Lamb, L. D.; Fostiropoulos, K.; Huffman, D. R. *Nature* **1990**, *347*, 354–358.
- Kobayashi, K.; Sano, Y.; Nagase, S. *J. Comput. Chem.* **2001**, *13*, 1353–1358. (b) Campanera, J. M.; Bo, C.; Olmstead, M. M.; Balch, A. L.; Poblent, J. M. *J. Phys. Chem. A* **2002**, *106*, 12356–12364.

- Lee, H. M.; Olmstead, M. M.; Iezzi, E.; Duchamp, J. C.; Dorn, H. C.; Balch, A. L. *J. Am. Chem. Soc.* **2002**, *124*, 3494–3495. (b) Maeda, Y.; et al. *J. Am. Chem. Soc.* **2004**, *126*, 6858–6859. (c) Cardona, C. M.; Kitaygorodskiy, A.; Ortiz, A.; Herranz, M. A.; Echegoyen, L. *J. Org. Chem.* **2005**, *70*, 5092–5097. (d) Cao, B.; Wakahara, T.; Maeda, Y.; Han, A.; Akasaka, T.; Kato, T.; Kobayashi, K.; Nagase, S. *Chem.—Eur. J.* **2004**, *10*, 716–720. (e) Kareev, I. E.; Lebedkin, S. F.; Bubnov, V. P.; Yagubskii, E. B.; Ioffe, I. N.; Khayre, P. A.; Kuvyichko, I. V.; Strauss, S. H.; Boltalina, O. V. *Angew. Chem. Int. Ed.* **2005**, *44*, 2–5.
- The Chemistry of Organic Silicon Compounds*; Patai, S., Rappoport, Z., Eds.; Wiley: Chichester, U.K., 1989.
- Wakahara, T.; Maeda, Y.; Kako, M.; Akasaka, T.; Kobayashi, K.; Nagase, S. *J. Organomet. Chem.* **2003**, *685*, 177–188. (b) Wakahara, T.; Kako, M.; Maeda, Y.; Akasaka, T.; Kobayashi, K.; Nagase, S. *Curr. Org. Chem.* **2003**, *7*, 927–943.
- Ando, W.; Kako, M.; Akasaka, T.; Nagase, S. *Organometallics* **1993**, *12*, 1514–1522 and references therein. (b) Masamune, S.; Murakami, S.; Tobita, H.; Williams, D. J. *J. Am. Chem. Soc.* **1983**, *105*, 7776–7778.

viewpoint of redox potentials and HOMO/LUMO levels.¹² The photochemical reaction of $\text{Sc}_3\text{N}@C_{80}$ with disilirane affords the adduct as a bis-silylated product.

We now report the full characterization of the bis-silylated $\text{Sc}_3\text{N}@C_{80}$ by means of NMR, vis–near-IR absorption and CV spectroscopy, and single-crystal X-ray structure analysis. In particular, we describe the dynamic behaviors of the disilirane moiety and the encapsulated Sc_3N cluster. Density functional calculations were also carried out for the $\text{Sc}_3\text{N}@C_{80}$ derivatives.

Experimental Section

Preparation and Purification of $\text{Sc}_3\text{N}@C_{80}$. The soot containing scandium metallofullerenes was prepared according to the reported procedure using a composite anode which contained graphite and scandium oxide with the atomic ratio of Sc/C equal to 0.8%.⁴ The composite rod was subjected to an arc discharge as an anode under a helium atmosphere that contained a small amount of N_2 gas. The raw soot containing scandium metallofullerenes was collected and extracted with 1,2,4-trichlorobenzene (TCB) solvent for 15 h. $\text{Sc}_3\text{N}@C_{80}$ was isolated from various empty fullerenes and other scandium metallofullerenes by a multistage high-performance liquid chromatography (HPLC) method. In the first stage, a 5PBB column (20 mm \times 250 mm i.d.; Cosmosil, Nacalai Tesque, Inc.) was used with TCB as eluent. In the second stage, a Buckyprep column (20 mm \times 250 mm i.d.; Cosmosil, Nacalai Tesque, Inc.) was used with toluene as eluent. Finally, in the third stage, a Buckyclutcher column (21 mm \times 500 mm i.d.; Regis Chemical) was used with toluene as eluent.

Bis-Silylation of $\text{Sc}_3\text{N}@C_{80}$. A 23 mL solution of $\text{Sc}_3\text{N}@C_{80}$ (4.6 mg, 4.1×10^{-6} mol) and disilirane (113 mg, 2.1×10^{-4} mol) in toluene/TCB (3/1) was placed in a Pyrex tube (20 mm i.d.), degassed by freeze–pump–thaw cycles under reduced pressures, and then irradiated with a Halogen lamp (cutoff < 400 nm) for 5 h. The adducts (**1A**, **1B**) were easily isolated from the unreacted disilirane and $\text{Sc}_3\text{N}@C_{80}$ by preparative HPLC using a Buckyprep column.

$\text{Sc}_3\text{N}@C_{80}(\text{Mes}_2\text{Si})_2\text{CH}_2\text{-A}$ (1A**):** ¹H NMR (300 MHz, $\text{CD}_2\text{Cl}_2/\text{CS}_2$, 293 K) δ 7.03 (s, 2H), 6.66 (s, 2H), 6.36 (s, 2H), 6.28 (s, 2H), 2.99 (s, 6H), 2.91 (d, $J = 13$ Hz, 1H), 2.48 (s, 6H), 2.31 (s, 6H), 2.17 (s, 6H), 1.99 (s, 6H), 1.99 (s, 6H), 1.86 (d, $J = 13$ Hz, 1H); ¹³C NMR (75 MHz, $\text{CD}_2\text{Cl}_2/\text{CS}_2$, 233 K) δ 157.8(2), 155.7(1), 155.4(1), 154.6(2), 150.9(2), 149.6(2), 149.2(2), 148.9(2), 147.3(2), 146.7(2), 144.7(2), 144.2(2), 144.1(2), 144.0(2), 144.0(2), 143.6(2), 142.7(2), 142.7(2), 142.0(2), 141.3(2), 141.2(2), 140.7(2), 140.4(2), 139.8(1), 139.2(1), 139.1(2), 138.9(2), 138.8(2), 138.0(2), 137.8(2), 137.8(2), 137.6(2), 137.4(2), 137.3(2), 137.0(2), 137.0(1), 135.9(2), 135.1(2), 134.8(2), 134.2(2), 132.8(2), 132.8(2), 132.3(2), 132.1(1), 131.8(2), 131.5(2), 130.2(2), 130.1(2), 130.0(2), 129.4(2), 128.6(2), 127.7(2), 127.5(2),

112.9(1), 107.9(1), 50.6(2), 30.5(2), 26.6(2), 26.1(2), 23.4(2), 20.9(2), 20.4(2), 3.2(2).

$\text{Sc}_3\text{N}@C_{80}(\text{Mes}_2\text{Si})_2\text{CH}_2\text{-B}$ (1B**):** vis–near-IR (CS_2) λ_{max} 900 nm; MALDI-TOF MS m/z 1655 (M^-), 1109 ($\text{M}^- - [(\text{Mes}_2\text{Si})_2\text{CH}_2]$).

$\text{Sc}_3\text{N}@C_{80}(\text{Mes}_2\text{Si})_2\text{CH}_2\text{-B-I}$ (1B-I**):** ¹H NMR (300 MHz, $\text{CDCl}_3/\text{CS}_2$, 233 K) δ 6.89 (s, 2H), 6.66 (s, 2H), 6.60 (s, 2H), 6.60 (s, 2H), 3.24 (s, 6H), 2.44 (s, 6H), 2.29 (s, 6H), 2.26 (s, 6H), 2.10 (s, 6H), 2.00 (s, 2H), 1.87 (s, 6H); ¹³C NMR (75 MHz, $\text{CD}_2\text{Cl}_2/\text{CS}_2$, 233 K) δ 176.4(2), 165.6(2), 152.7(2), 152.3(2), 152.2(2), 150.7(2), 149.5(2), 147.2(2), 146.7(2), 146.7(2), 146.5(2), 145.7(2), 145.7(2), 145.1(2), 144.7(2), 144.5(2), 143.1(2), 142.4(2), 142.3(2), 141.4(2), 140.7(2), 140.7(2), 140.5(2), 140.0(2), 139.8(2), 139.7(2), 139.1(2), 138.4(2), 138.4(2), 138.2(2), 137.6(2), 135.4(2), 135.2(2), 134.9(2), 134.7(2), 134.2(2), 133.7(2), 133.4(2), 133.2(2), 132.8(2), 132.5(2), 132.2(2), 131.1(2), 130.1(2), 130.0(2), 129.9(2), 128.7(2), 128.4(2), 128.3(2), 128.2(2), 114.8(2), 56.8(2), 30.6(2), 29.1(2), 28.6(2), 25.9(2), 25.5(2), 21.4(2), 11.3(2).

$\text{Sc}_3\text{N}@C_{80}(\text{Mes}_2\text{Si})_2\text{CH}_2\text{-B-II}$ (1B-II**):** ¹H NMR (300 MHz, $\text{CDCl}_3/\text{CS}_2$, 233 K) δ 6.83 (s, 2H), 6.81 (s, 2H), 6.66 (s, 2H), 6.60 (s, 2H), 3.10 (s, 6H), 2.55 (s, 6H), 2.37 (s, 6H), 2.29 (s, 6H), 2.21 (s, 6H), 2.17 (s, 2H), 1.92 (s, 6H); ¹³C NMR (125 MHz, $\text{CD}_2\text{Cl}_2/\text{CS}_2$, 233 K) δ 179.9(2), 152.4(2), 151.7(2), 151.2(2), 150.9(2), 149.4(2), 146.9(2), 146.7(2), 146.6(2), 146.2(2), 145.4(2), 145.3(2), 144.9(2), 144.9(2), 144.0(2), 142.9(2), 142.9(2), 142.8(2), 141.9(2), 141.2(2), 140.8(2), 140.6(2), 140.4(2), 140.3(2), 140.1(2), 139.9(2), 139.9(2), 138.8(2), 138.2(2), 138.2(2), 138.1(2), 138.0(2), 138.0(2), 135.5(2), 135.4(2), 134.8(2), 134.5(2), 134.5(2), 134.0(2), 134.0(2), 133.8(2), 133.2(2), 132.5(2), 132.1(2), 131.6(2), 130.5(2), 130.5(2), 129.0(2), 128.4(2), 128.0(2), 116.9(2), 57.3(2), 28.2(2), 25.8(2), 25.2(2), 23.8(2), 23.7(2), 21.1(2), 11.5(2).

Black crystals of **1B** were obtained by layering a solution of **1B** in 3.0 mL of CS_2 on the bottom of 9.0 mL of hexane, in a glass tube (7.0 mm i.d.) at 273 K. The crystal data are as follows: $\text{mf} = \text{C}_{117}\text{H}_{46}\text{NSc}_3\text{Si}_2$; $\text{fw} = 1656.61$; black plate; tetragonal, space group $I4_1$ (No. 80); $a = 20.4678(14)$, $b = 20.4678(14)$, $c = 15.804(2)$ Å; $V = 6620.8(12)$ Å³; $Z = 4$; $D_{\text{calc}} = 1.662$ g cm^{-3} ; $\mu(\text{Mo K}\alpha) = 0.656$ mm⁻¹; $\theta = 2.22$ – 27.70° ; $T = 90$ K; $R_1 = 0.1501$, $wR_2 = 0.3804$ for all data; $R_1 = 0.1474$ for 7576 reflections ($I > 2.0\sigma(I)$) and 757 parameters. The maximum residual electron density is equal to 0.821 e Å⁻³.

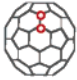
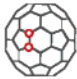
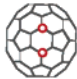
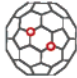
Toluene was distilled over benzophenone sodium ketyl under an argon atmosphere prior to use. 1,2-Dichlorobenzene was distilled over P_2O_5 under vacuum prior to use. HPLC isolation was performed on a LC-908 (Japan Analytical Industry Co., Ltd.). Toluene was used as the eluent, and the eluants were monitored by the UV absorption at 330 nm. Mass spectrometry was performed on a Bruker BIFLEX III with 9-nitroanthracene as matrix. Absorption spectra were measured by using a Shimadzu UV-3150. The ¹H, ¹³C, ¹H–¹H COSY, HMQC, HMBC, and 2D EXCY NMR spectra were measured on a Bruker Avance-300, Avance-500, and Avance-600 spectrometers. Cyclic voltammograms (CV) and differential pulse voltammograms (DPV) were recorded on a BAS CV50W electrochemical analyzer. A platinum disk and a platinum wire were used as the working electrode and the counter electrode, respectively. The reference electrode was a saturated calomel reference electrode (SCE) filled with 0.1 M $n\text{-Bu}_4\text{NPF}_6$ in 1,2-dichlorobenzene. All potentials are referenced to the ferrocene/ferrocenium couple (Fc/Fc^+) as the standard. CV: scan rate, 20 mV/s. DPV: pulse amplitude, 50 mV; pulse width, 50 ms; pulse period, 200 ms; scan rate, 20 mV/s.

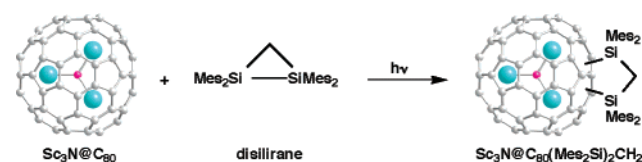
Theoretical Calculations. Geometries were optimized with hybrid density functional theory at the B3LYP^{13–15} level using the Gaussian 03 program.¹⁶ The effective core potential and the corresponding basis

- (11) Akasaka, T.; Kato, T.; Kobayashi, K.; Nagase, S.; Yamamoto, K.; Funasaka, H.; Takahashi, T. *Nature* **1995**, *374*, 600–601. (b) Wakahara, T.; Kobayashi, J.; Yamada, M.; Maeda, Y.; Tsuchiya, T.; Okamura, M.; Akasaka, T.; Waelchli, M.; Kobayashi, K.; Nagase, S.; Kato, T.; Kako, M.; Yamamoto, K.; Kadish, K. M. *J. Am. Chem. Soc.* **2004**, *126*, 4883–4887. (c) Akasaka, T.; Okubo, S.; Kondo, M.; Maeda, Y.; Wakahara, T.; Kato, T.; Suzuki, T.; Yamamoto, K.; Kobayashi, K.; Nagase, S. *Chem. Phys. Lett.* **2000**, *319*, 153–156. (d) Akasaka, T.; Nagase, S.; Kobayashi, K.; Suzuki, T.; Kato, T.; Yamamoto, K.; Funasaka, H.; Takahashi, T. *J. Chem. Soc., Chem. Commun.* **1995**, 1343–1344. (e) Akasaka, T.; Nagase, S.; Kobayashi, K.; Suzuki, T.; Kato, T.; Kikuchi, K.; Achiba, Y.; Yamamoto, K.; Funasaka, H.; Takahashi, T. *Angew. Chem., Int. Ed. Engl.* **1995**, *34*, 2139–2141. (f) Wakahara, T.; Sakuraba, A.; Iiduka, Y.; Okamura, M.; Tsuchiya, T.; Maeda, Y.; Ishizuka, M. O.; Akasaka, T.; Okubo, S.; Kato, T.; Kobayashi, K.; Nagase, S.; Kadish, K. M. *Chem. Phys. Lett.* **2004**, *398*, 553–555. (g) Yamada, M.; Feng, L.; Wakahara, T.; Tsuchiya, T.; Maeda, Y.; Lian, Y.; Kako, M.; Akasaka, T.; Kato, T.; Kobayashi, K.; Nagase, S. *J. Phys. Chem. B* **2005**, *109*, 6049–6051. (h) Yamada, M.; Nakahodo, T.; Wakahara, T.; Tsuchiya, T.; Maeda, Y.; Akasaka, T.; Kako, M.; Yoza, K.; Horn, E.; Mizorogi, N.; Kobayashi, K.; Nagase, S. *J. Am. Chem. Soc.* **2005**, *127*, 14570–14571.
- (12) Iiduka, Y.; Ikenaga, O.; Sakuraba, A.; Wakahara, T.; Tsuchiya, T.; Maeda, Y.; Nakahodo, T.; Akasaka, T.; Kako, M.; Mizorogi, N.; Nagase, S. *J. Am. Chem. Soc.* **2005**, *127*, 9956–9957.

- (13) Becke, A. D. *Phys. Rev. A* **1988**, *38*, 3098–3100.
 (14) Becke, A. D. *J. Chem. Phys.* **1993**, *98*, 5648–5652.
 (15) Lee, C.; Yang, W.; Parr, R. G. *Phys. Rev. B* **1988**, *37*, 785–789.
 (16) Frisch, M. J.; et al. GAUSSIAN 03, revision C. 01; Gaussian Inc.: Wallingford, CT, 2004.

Table 1. Isomers and Their Symmetries of C₈₀(Mes₂Si)₂CH₂

isomer	site	form	conformation	symmetry	equivalency of CH ₂ Si C(○)	Me	¹³ C NMR pattern of C ₈₀ cage sp ²	sp ³
1,2(ab)		open	planar	C _s	○ × ×	6H×6	2C×36, 1C×8	—
			bent	C ₁	× × ×	3H×12	1C×80	—
			twist	C ₁	× × ×	3H×12	1C×80	—
		closed	planar	C _s	○ × ×	6H×6	2C×36, 1C×6	1C×2
			bent	C ₁	× × ×	3H×12	1C×78	1C×2
			twist	C ₁	× × ×	3H×12	1C×78	1C×2
1,2(aa)		open	planar	C _s	× ○ ○	6H×6	2C×36, 1C×8	—
			bent	C _s	× ○ ○	6H×6	2C×36, 1C×8	—
			twist	C ₁	× × ×	3H×12	1C×80	—
		closed	planar	C _s	× ○ ○	6H×6	2C×35, 1C×8	2C×1
			bent	C _s	× ○ ○	6H×6	2C×35, 1C×8	2C×1
			twist	C ₁	× × ×	3H×12	1C×78	1C×2
1,4(bb)		planar	C _{2v}	○ ○ ○	12H×3	4C×16, 2C×7	2C×1	
		bent	C _s	× ○ ○	6H×6	2C×36, 1C×6	2C×1	
		twist	C ₂	○ ○ ○	6H×6	2C×39	2C×1	
1,4(aa)		planar	C ₂	○ ○ ○	6H×6	2C×39	2C×1	
		bent	C ₁	× × ×	3H×12	1C×78	1C×2	
		twist	C ₂	○ ○ ○	6H×6	2C×39	2C×1	

Scheme 1

set¹⁷ were used for Sc, and electrons in the outermost core orbitals were explicitly treated as valence electrons. The contraction scheme employed for the basis set was (5s5p5d)/[4s4p3d] for Sc in the standard notation. The split-valence d-polarized 6-31G(d)¹⁸ basis set was used for Si, C, N, and H.

Results and Discussion

Structural Determination of Sc₃N@C₈₀(Mes₂Si)₂CH₂-A (1A). As Scheme 1 shows, photolysis of a toluene/TCB (3/1) solution of disilirane and Sc₃N@C₈₀ led to the ready formation of the 1:1 adduct (**1**). The separation of the adduct was subsequently achieved using a HPLC on a Buckyprep column with toluene used as the eluent. The MALDI-TOF mass spectrum of the isolated **1** verified the formation of the 1:1 adduct.

The I_h structure of the C₈₀ fullerene has two kinds of nonequivalent carbon atoms. Therefore, there are two addition sites for each of the 1,2- and 1,4-cycloadditions: 1,2(aa), 1,2(ab); 1,4(aa) and 1,4(bb). The possible isomers and symmetries of C₈₀(Mes₂Si)₂CH₂ are shown in Table 1. The molecular symmetry of **1** was determined by means of NMR spectral analyses. The ¹H NMR spectrum of **1** indicates the presence of two isomers, **1A**,**B** (Figure 1a). From the peak areas it was estimated that the ratio of **1A** to **1B** is 3:2. These isomers could not be resolved by the HPLC method using a Buckyprep column

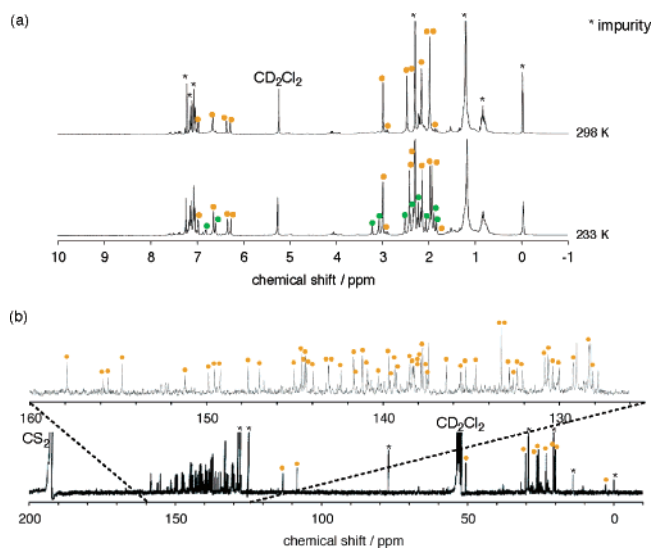


Figure 1. (a) ¹H (at 298, 233 K) and (b) ¹³C (at 233 K) NMR spectra of **1** in CD₂Cl₂ (right red, **1A**; green, **1B**).

because of their identical retention times. Six methyl signals and four *meta*-proton signals from the mesityl groups are assigned to **1A**. The ¹H–¹H COSY NMR spectrum of **1** shows four cross-peaks between two doubled signals of **1A**. These signals are assigned to the two methylene protons of **1A**, therefore, which are in nonequivalent environments. Accordingly, it is found that **1A** has C_s symmetry and the mirror plane passes through the two sp³ carbon atoms bonded to the disilirane moiety. The other signals are assigned to **1B**. However, it is not possible to assign completely the signals of **1B** because of the overlap with signals of **1A**. The ¹³C NMR spectrum of **1** shows 43 (35 × 2; 8 × 1) signals due to sp² carbon atoms and one signal due to the sp³ carbon atom for the C₈₀ skeleton of **1A** (Figure 1b). Twelve signals for four tertiary and eight

(17) Hay, P. J.; Wadt, W. R. *J. Chem. Phys.* **1985**, *82*, 299–310.

(18) Hehre, W. J.; Ditchfield, R.; Pople, J. A. *J. Chem. Phys.* **1972**, *56*, 2257–2261.

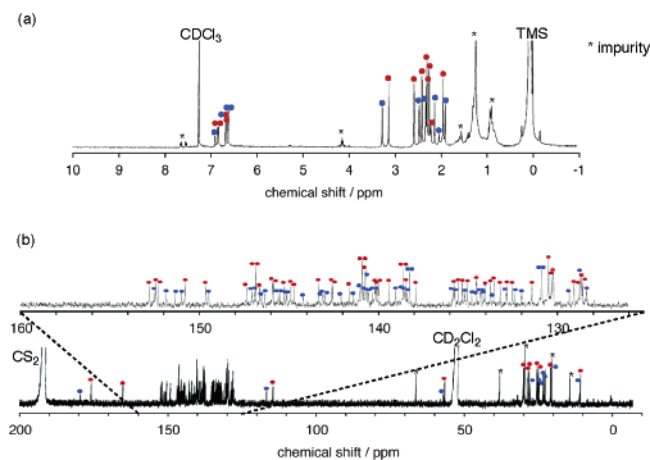


Figure 2. (a) ^1H (in $\text{CS}_2/\text{CDCl}_3$) and (b) ^{13}C (in $\text{CS}_2/\text{CD}_2\text{Cl}_2$) NMR spectra of **1B** at 233 K (red, **1B-I**; blue, **1B-II**).

quaternary aromatic carbon atoms and one signal for the methylene carbon atom of the disilirane moiety of **1A** were also observed. The signals of **1B** were not observed because of the relatively low intensity. The HMBC NMR spectrum gave crucial evidence for the identification of the 1,3-disilolane structure in **1A**; i.e., a cross-peak corresponding to one proton of methylene group at 1.86 ppm and two sp^3 carbon atoms of the C_{80} skeleton at 50.6 ppm was observed. These spectral data reveal that **1A** results from the addition of disilirane on the bond junction between 5- and 6-membered rings resulting in the formation of a closed structure (1,2(aa)-closed). Interestingly, no cross-peak corresponding to another methylene proton at 2.91 ppm and the sp^3 carbon atoms was observed. This implied that **1A** has a frozen (no ring inversion) conformer in the bent conformation on the NMR time scale. Although, two kinds of bent diastereomeric conformers are possible, the conformation cannot be deduced by NMR spectroscopy. We are currently trying to obtain single crystals suitable for X-ray structural analysis to verify the molecular structure.

Structural Determination of $\text{Sc}_3\text{N}@\text{C}_{80}(\text{Mes}_2\text{Si})_2\text{CH}_2\text{-B}$ (1B**).** A most interesting finding is that **1A** isomerizes thermally to **1B**. This means that the 1,2(aa)-adduct is thermodynamically less stable than the 1,4(aa)-adduct but is more favorable kinetically, as mentioned below. A mixture of **1A**, **B** was heated in 1,2-dichlorobenzene at 353 K for 80 min. After heating, the ^1H NMR spectrum shows two sets of 11 signals which can be assigned to **1B**, with a complete disappearance of signals due to **1A** (Figure 2a). **1B** is composed of two conformers (**1B-I** and **1B-II**), and the **1B-I/1B-II** ratio is 5/3. Six methyl signals, four *meta*-proton signals, and one methylene signal from the disilirane moiety were observed for each of **1B-I** and **1B-II**. The ^{13}C NMR spectrum of **1B** shows two sets of 39 signals of the C_{80} skeleton (Figure 2b). Twelve signals for four tertiary and eight quaternary aromatic carbon atoms and one signal for the methylene carbon atom of the disilirane moiety for each of **1B-I** and **1B-II** were also observed. The HMQC NMR spectrum shows one cross-peak corresponding to the methylene protons and the sp^3 carbon atoms for each of **1B-I** and **1B-II**. These spectral data suggest that **1B-I** and **1B-II** are due to the 1,4(aa)- or 1,4(bb)-adduct having the 1,3-disilipine structure with C_2 symmetry.

To determine the addition site of **1B**, VT- ^1H NMR measurements were carried out by varying temperatures from 243 to

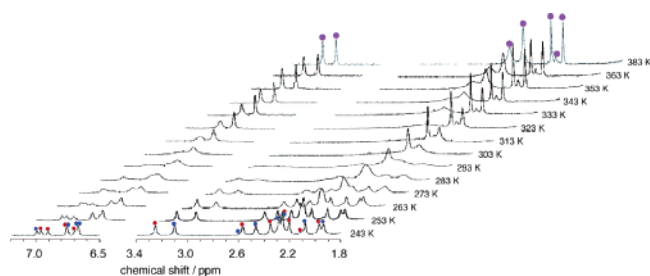


Figure 3. VT- ^1H NMR spectra of **1B** in 1,1,2,2-tetrachloroethane- d_2 .

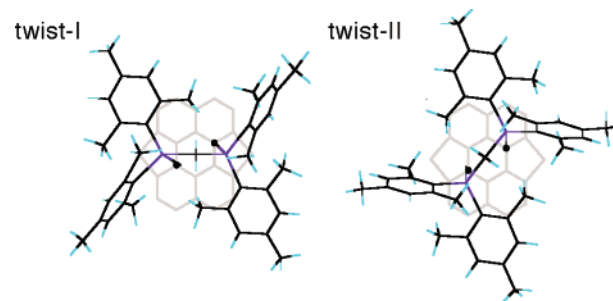


Figure 4. Two twist modes on conformations of the silyl group.

383 K at intervals of 10 K (Figure 3). The signals were sharp at 243 K and broad around 293 K, and above this temperature the line widths narrowed. Surprisingly, at 383 K the signals for **1B-I** and **1B-II** became equivalent with an intermediate chemical shift comparable to those for **1B-I** and **1B-II** at 243 K. After recoiling of the ^1H NMR sample to 243 K, the spectrum before heating was observed. This indicates that there is a chemical exchange between **1B-I** and **1B-II**. Two nonequivalent signals for *ortho*-methyl protons about one mesityl group became equivalent at 383 K, because the mesityl groups could rotate around their Si-C single covalent bond. The spectrum at 383 K indicates that **1B** has C_2 symmetry. Therefore, it was concluded that both **1B-I** and **1B-II** are 1,4(aa)-adducts. The 1,4(aa)-adduct has two twist conformers of the disilirane moiety, namely twist-I and twist-II, as shown in Figure 4. Hence, the observed chemical exchange between **1B-I** and **1B-II** can be attributable to the transformation from one twist conformer to another.

2D EXSY NMR measurement was acquired using the phase-sensitive NOESY pulse sequence to investigate the interrelation between **1B-I** and **1B-II**. The spectrum showed several cross-peaks corresponding to **1B-I** and **1B-II**, indicating a chemical exchange between **1B-I** and **1B-II** (Figure 5). To calculate the magnetization exchange rates k' of the exchange equilibrium ($k' = c(\text{mol/L}) \cdot k$), we carried out a quantitative analysis of the experimental intensities of the NMR peaks obtained in the 2D EXSY NMR experiments. In particular, 2D EXSY NMR spectra were measured at 223, 233, and 243 K and at a mutually equal concentration (c). The k' 's calculated at 223, 233, and 243 K are 1.11, 3.91, and 13.63, respectively. The activation energy ΔG^\ddagger for the transformation from **1B-I** to **1B-II** was estimated as 13.5 kcal/mol from an Arrhenius plot. The energy difference, ΔG , between **1B-I** and **1B-II** was estimated to be 0.2 kcal/mol according to the Boltzmann distribution. For $\text{C}_{60}(\text{Dep}_2\text{Ge})_2\text{CH}_2$ (1,4-adduct, Dep = 2,6-diethylphenyl), the corresponding activation energy is 17.8 kcal/mol.¹⁹

(19) Akasaka, T.; et al. *Org. Lett.* **2000**, *2*, 2671–2674.

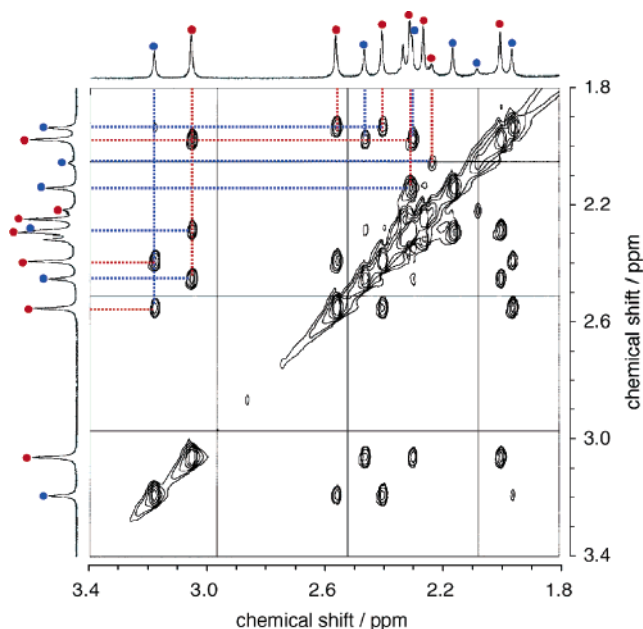


Figure 5. 2D EXSY NMR spectrum of **1B** in $\text{CS}_2/\text{CDCl}_3$ at 233 K (red, **1B-I**; blue, **1B-II**).

The structure of **1B** was confirmed by single-crystal X-ray structure analysis. At 90 K the two conformers, **1B-I** and **1B-II**, are disordered on a common site with occupancies equal to 0.70 and 0.30, respectively (Figure 6). The occupancy ratio is consistent with that determined from the ^1H NMR measurement

at 233 K. Certainly, **1B-I** and **1B-II** correspond to twist-I and twist-II structures, respectively. The encapsulated Sc_3N cluster in both **1B-I** and **1B-II** is located at a single site and at the same mutual position. This suggests that the free circular motion of the Sc_3N cluster in pristine $\text{Sc}_3\text{N}@C_{80}$ is restricted in the silylated adduct.

The details of the molecular structures of **1B-I** and **1B-II** are as follows. The Si–C bond ($\text{Si}(1)–\text{C}(1) = 2.003 \text{ \AA}$) between the disilirane moiety and the C_{80} cage is elongated compared with the distances usually found in alkylsilane compounds. This elongation may be due to the steric repulsion between the bulky mesityl groups and the C_{80} cage and the silicon β -effect by $\sigma-\pi$ conjugation between the σ -orbital of Si–C bonds and the π -orbital of the C_{80} cage. In both **1B-I** and **1B-II**, Sc(1) is located near the hexagon on the bottom with $\text{Sc}(1)–\text{C}(2) = 2.379 \text{ \AA}$, $\text{Sc}(1)–\text{C}(3) = 2.394 \text{ \AA}$, and $\text{Sc}(1)–\text{C}(4) = 2.408 \text{ \AA}$. In **1B-I**, Sc(2) is located over a 5–6 bond with the $\text{Sc}(2)–\text{C}(5) = 2.190 \text{ \AA}$ and $\text{Sc}(2)–\text{C}(6) = 2.273 \text{ \AA}$. In **1B-II**, Sc(3) is also located over a 5–6 bond with the $\text{Sc}(3)–\text{C}(9) = 2.133 \text{ \AA}$ and $\text{Sc}(3)–\text{C}(10) = 2.304 \text{ \AA}$. The Sc_3N cluster is planar with the sum of N–Sc bond angles of 360.0 and 360.1° for **1B-I** and **1B-II**, respectively. The N–Sc distances ($\text{N}(1)–\text{Sc}(1) = 1.989 \text{ \AA}$, $\text{N}(1)–\text{Sc}(2) = 2.022 \text{ \AA}$, and $\text{N}(1)–\text{Sc}(3) = 2.007 \text{ \AA}$) are almost the same as those in $(\text{Sc}_3\text{N}@C_{80})\cdot\text{Co}^{\text{II}}(\text{OEP})\cdot 1.5\text{CHCl}_3\cdot 0.5\text{C}_6\text{H}_6$ ($1.966\text{--}2.011 \text{ \AA}$)⁴ and $\text{Sc}_3\text{N}@C_{80}\text{--}C_{10}\text{H}_{12}\text{O}_2$ ($2.020\text{--}2.032 \text{ \AA}$).^{7a} The C(7)–C(8) bond length (1.339 \AA) of the hexagonal ring, which connects with the disilirane moiety, is shorter than other C–C bond lengths of the C_{80} cage. This

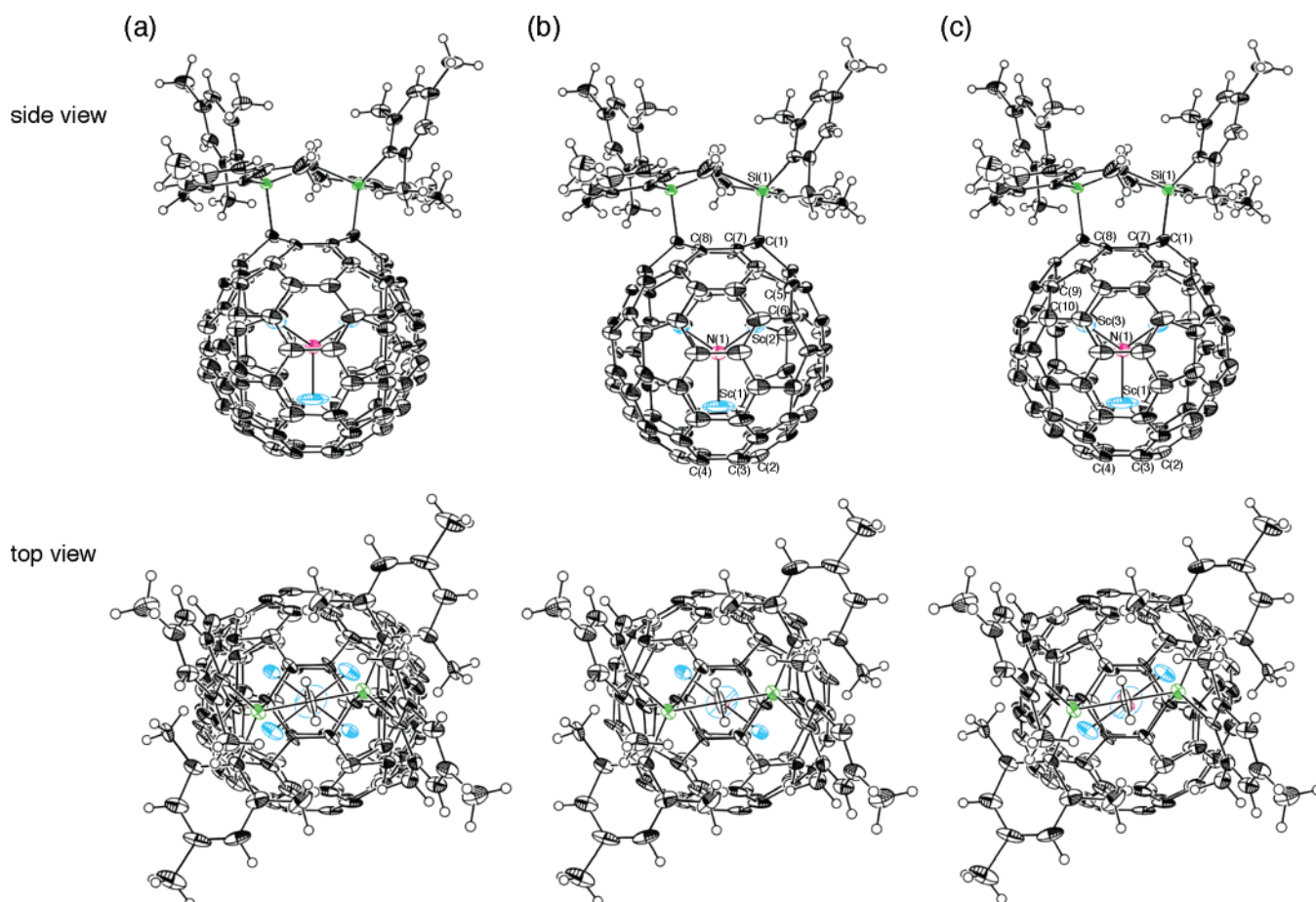


Figure 6. ORTEP drawings of (a) **1B**, (b) **1B-I**, and (c) **1B-II** showing thermal ellipsoid at the 50% probability level.

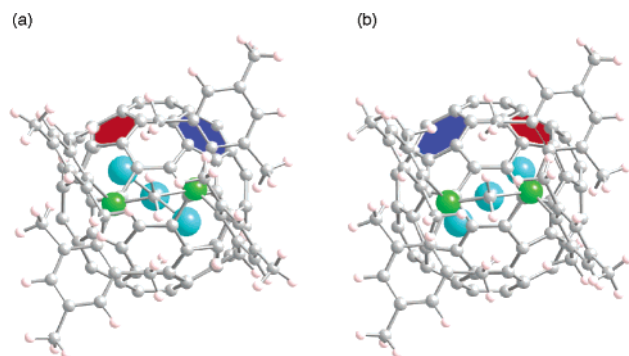


Figure 7. Optimized structures of (a) **1B-I** and (b) **1B-II**.

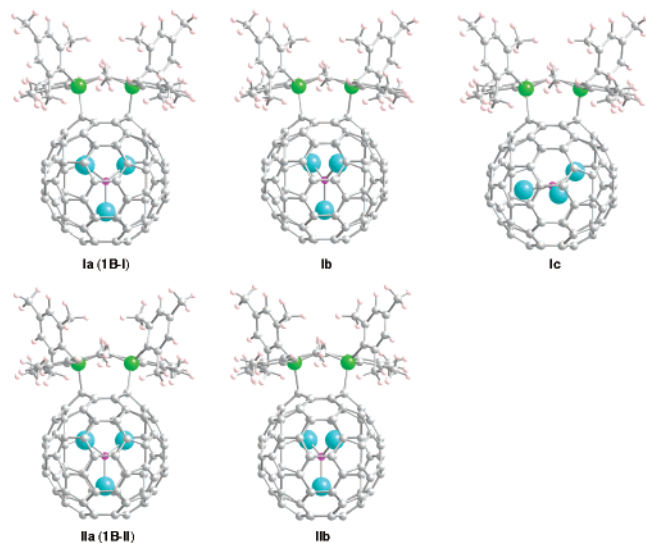


Figure 8. Optimized structure of $\text{Sc}_3\text{N}@C_{80}(\text{Mes}_2\text{Si})_2\text{CH}_2$.

indicates that the double bond character of the C(7)–C(8) bond is enhanced by addition of the disilirane moiety.

Theoretical Calculations. Full geometry optimization was carried out for **1B**. Figure 7 shows the optimized structures of **1B-I** and **1B-II** with C_2 symmetry. **1B-I** and **1B-II** are almost isoenergetic, **1B-I** being only 0.6 kcal/mol less stable than **1B-II**. Figure 8 shows the structures of $\text{Sc}_3\text{N}@C_{80}(\text{Mes}_2\text{Si})_2\text{CH}_2$ optimized by changing the positions of the Sc_3N cluster. For three twist-I structures, **Ia–c**, the positions of the Sc atoms are different. **Ia (1B-I)** is 5.6 and 13.8 kcal/mol more stable than **Ib** and **Ic**, respectively. For two twist-II structures, **IIa (1B-II)** is 17.8 kcal/mol more stable than **IIb**. This result suggests that the Sc_3N cluster in the bis-silylated $\text{Sc}_3\text{N}@C_{80}$ cannot rotate freely. In contrast, the Sc_3N cluster in the pristine $\text{Sc}_3\text{N}@C_{80}$ rotates rather freely, because the electrostatic potential map calculated inside the I_h cage of C_{80}^{6-} shows almost concentric circles along the cage with no clear minima, reflecting its round cage structure.⁶ However, the electrostatic potential maps for **1B-I** and **1B-II** are modified by the silyl addition. Recently, we have found that two Ce atoms in $\text{Ce}_2@C_{80}(\text{Mes}_2\text{Si})_2\text{CH}_2$ (1,4(aa)-adduct) were positioned on the equator plane with respect to the disilirane moiety.^{11h} Interestingly, the theoretical calculation reveals that the free random motion of the Sc_3N cluster in $\text{Sc}_3\text{N}@C_{80}$ is fixed in the perpendicular plane to the equator by attaching disilirane.

Electronic Property of 1B. The change of the electrostatic potential map inside the C_{80} cage is due to the electron-donating

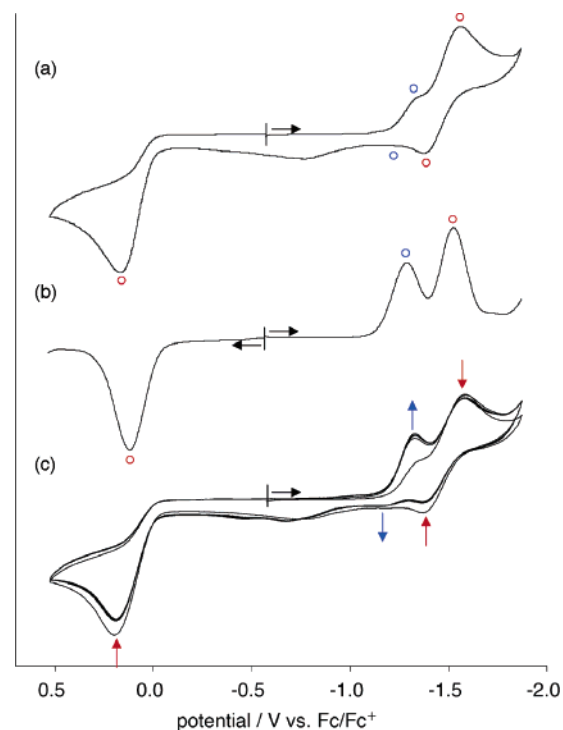


Figure 9. (a) CV, (b) DPV, and (c) multiscan CV spectra of **1B** (red circle and arrow). Peaks assigned to $\text{Sc}_3\text{N}@C_{80}$ are indicated by the blue circle and arrow.

Table 2. Redox Potentials^a (V) and HOMO/LUMO Levels (eV) of **1B** and $\text{Sc}_3\text{N}@C_{80}$

compd	${}^{\circ}\text{E}_1$	${}^{\circ}\text{E}_1$	HOMO	LUMO
1B				
1B-I			-4.79	-2.81
1B-II	+0.08 ^b	-1.45	-4.81	-2.78
$\text{Sc}_3\text{N}@C_{80}$ ^c	+0.62	-1.22	-5.48	-3.14

^a Half-cell potentials unless otherwise stated. Values are relative to the ferrocene/ferrocenium couple. ^b Irreversible. Values were obtained by DPV. Conditions: working electrode and counter electrode, Pt wire; reference electrode, SCE; supporting electrolyte, 0.1 M *n*-Bu₄NPF₆ in 1,2-dichlorobenzene. CV: scan rate, 20 mV/s. DPV: pulse amplitude, 50 mV; pulse width, 50 ms; pulse period, 200 ms; scan rate, 20 mV/s. ^c Reference 11.

nature of disilirane. The redox potentials of **1B** were measured by CV and DPV (Figure 9). Interestingly, the desilylation process took place during the measurement. The multiscan CV spectrum shows that the reduction wave corresponding to the parent $\text{Sc}_3\text{N}@C_{80}$ becomes more intensive, while the reduction wave corresponding to **1B** becomes much weaker, as shown in Figure 9c. After the CV measurement, the HPLC profile shows a peak due to the parent $\text{Sc}_3\text{N}@C_{80}$ as well as **1B**. This indicates that the disilirane moiety is eliminated under CV and DPV conditions, so we can control its addition and elimination. Since the fullerene cages of silylated metallofullerenes are electron rich as a result of the electron donation from the disilirane moiety, the first reduction potential of **1B** was cathodically shifted to 230 mV, and the first oxidation potential was also cathodically shifted to 540 mV, as in the case of $\text{M}@C_{82}$ ($\text{M} = \text{Y}$ and La).^{11g} Furthermore, the first and second reduction potentials correlate well with the LUMO energy levels, and the oxidation potentials also correlate with the HOMO levels. As shown in Table 2, the HOMO/LUMO levels of **1B-I**, **1B-II**, and $\text{Sc}_3\text{N}@C_{80}$ are -4.79/-2.81, -4.81/-2.78, and -5.48/-3.14 eV, respectively. In this context, it is worthy to note that

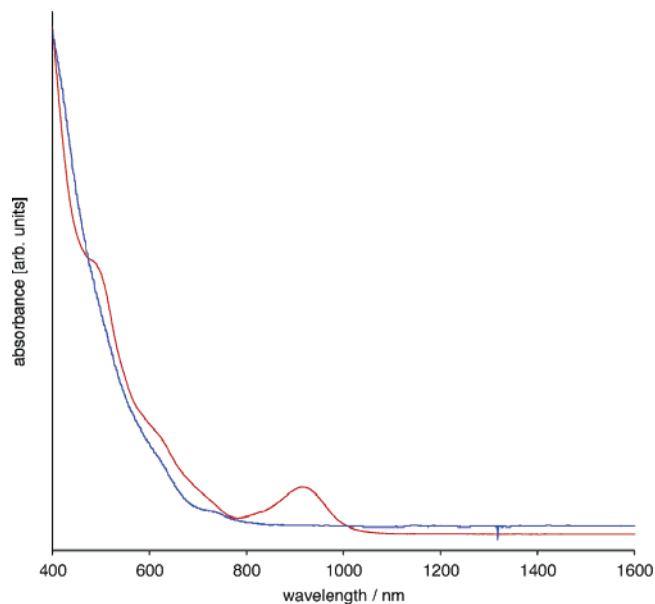


Figure 10. Visible–near-IR absorption spectra of **1B** (red line) and $\text{Sc}_3\text{N@C}_{80}$ (blue line).

the silylated $\text{Sc}_3\text{N@C}_{80}$ have the smaller HOMO–LUMO gap than the pristine $\text{Sc}_3\text{N@C}_{80}$. The increase of the HOMO levels is caused by the electron-donating group. It was calculated that a considerable charge transfer takes place from the disilirane moiety to $\text{Sc}_3\text{N@C}_{80}$, giving an electronic structure described as $(\text{Sc}_3\text{N@C}_{80})^{1.2-}((\text{Mes}_2\text{Si})_2\text{CH}_2)^{1.2+}$.

The vis–near-IR absorption spectrum of **1B** in CS_2 shows an absorption maximum at 900 nm (Figure 10). The difference in the absorption spectrum between $\text{Sc}_3\text{N@C}_{80}$ and **1B** demonstrates that the π electronic state of the C_{80} cage is changed by the silylation. These results reveal that silylation is effective for tuning the electronic character of $\text{Sc}_3\text{N@C}_{80}$, as well as the empty fullerenes and M@C_{82} .^{11g}

Conclusions

Both 1,2- and 1,4-cycloadducts were successfully isolated and completely characterized by NMR measurement and single-crystal X-ray structure analysis. Experimental results and theoretical calculations reveal that the circular motion of Sc_3N cluster in $\text{Sc}_3\text{N@C}_{80}$ is restricted by exohedral addition.

Acknowledgment. Y.I. thanks the Japan Society for the Promotion of Science (JSPS) for the Research Fellowship for Young Scientists. This work was supported in part by a Grant-in-Aid, the 21st Century COE Program, Nanotechnology Support Project, NAREGI Nanoscience Project from the Ministry of Education, Culture, Sports, Science, and Technology of Japan, and a grant from the Kurata Memorial Hitachi Science and Technology Foundation.

Supporting Information Available: X-ray crystallographic details including the crystallographic information file (CIF) and complete refs 7b, 16, and 19. This material is available free of charge via the Internet at <http://pubs.acs.org>.

JA062233H